ARMA 23–0014

3DEC Simulations of Dynamic Direct Shear Tests Considering Joint Roughness Coefficient (JRC)

Kim, B.H. and M.K. Larson
CDC/NIOSH, Spokane, Washington, United States

This paper was prepared for presentation at the 57th US Rock Mechanics/Geomechanics Symposium held in Atlanta, Georgia, USA, 25-28 June 2023. This paper was selected for presentation at the symposium by an ARMA Technical Program Committee based on a technical and critical review of the paper by a minimum of two technical reviewers. The material, as presented, does not necessarily reflect any position of ARMA, its officers, or members. Electronic reproduction, distribution, or storage of any part of this paper for commercial purposes without the written consent of ARMA is prohibited. Permission to reproduce in print is restricted to an abstract of not more than 200 words; illustrations may not be copied. The abstract must contain conspicuous acknowledgement of where and by whom the paper was presented.

ABSTRACT: In general, the dynamic properties, e.g., dynamic rock modulus and dynamic rock (shear or tensile) strength are two to three times greater than static moduli and strengths. Thus, understanding the dynamic rock characteristics is necessary to improve the design of support systems in underground mines, nearly all of which are subject to dynamic loading. In this paper, we report the baseline results of an ongoing study. Experimental direct shear tests were conducted on jointed specimens that were created by 3D printer to represent 3D joint roughness coefficients (JRCs) of 12 and 17. These JRC values are relatively close, but they represent the roughness of a large proportion of joints found in underground mines. We also report the results of numerical direct shear tests using 3DEC modeling code that were conducted for the purpose of learning more about dynamic shear failure mechanisms. We performed static direct shear tests for the purpose of calibrating our models with the empirical solution. Results of these tests compared well with the empirical results. Subsequent dynamic numerical direct shear tests were performed using 3DEC, simulating the dynamic direct shear tests performed in the laboratory. The numerical direct shear stresses compared well with those of the laboratory tests. Furthermore, the results confirm that the ratio of dynamic to static shear strengths vary between approximately 2 and 3 in the range of normal stresses used in the tests.

1. INTRODUCTION

Dynamic failure in coal mines, known as “bursts” or “bumps,” is one of the most challenging and persistent engineering problems associated with coal mining in highly stressed conditions. These events occur when stresses in a coal pillar, used for support in underground workings, exceed the critical strength of the pillar, causing the pillar to rupture without warning. These events can be exceptionally violent, ejecting coal and rock with explosive force [*1, 2*].

These events occur suddenly and often without warning. As such, miners often do not have the opportunity to move to safety before an event. Although relatively rare, dynamic failure events resulted in worker injury up to and including fatality in 52% of the reported cases occurring from 2000–2019. Moreover, the fatality rate is roughly ten times greater than that associated with roof falls, a leading cause of ground-control-related injuries in underground coal mines [*3*]. The risk associated with faults/fault zones and coal bumps has been acknowledged by several researchers in the literature. Mauck [*4*] and Peperakis [*5*] mention the risk of bumps with regard to the proximity of mining operations to faults. Some describe the role of faults in stress concentration [*5-9*], thus causing conditions with increased bursts/bumps risk. Others specifically mention fault slip and the resulting release of energy associated with bursts/bumps [*5, 7-10*].

However, conventional rock support designs that only consider static loading are inadequate to safely maintain underground excavations under dynamic loading because dynamic properties are very different from static properties of a rock mass. In general, the dynamic properties, e.g., dynamic rock modulus and dynamic rock (shear or tensile) strength, are two to three times greater than static moduli and strengths. Thus, understanding the dynamic rock characteristics is necessary to improve the design of support systems in underground mines, nearly all of which are subject to dynamic loading

This paper is part of an effort by the National Institute for Occupational Safety and Health (NIOSH) to identify risk factors associated with bursts/bumps in highly stressed ground conditions. More specifically, this paper reports the baseline results of an ongoing study. Based on the experimental direct shear tests on jointed specimens manufactured by 3D printer to represent 3D joint roughness coefficients (JRC) [*11*], we report the results of numerical direct shear tests using 3DEC modeling code [*12*] that were conducted for the purpose of learning more about dynamic shear failure mechanisms.

This paper describes common approaches for a joint shear deformation analysis by direct shear test simulation under both static and dynamic loading. A 3-dimensional block model of a laboratory-scale specimen was constructed for the direct shear test using 3DEC. After the completion of the direct shear test simulations, a shear stress of the joint surface for each test was estimated by back calculation.

2. METHODS

For the direct shear simulation in this study, the 3DEC model was built in a 3D-dimension with 0.06 (W) x 0.13 (L) x 0.03 m (D) as big as the laboratory specimen. To create the two different joint surface geometries, we considered the joint roughness coefficient (JRC) and the replication techniques of the geometries published in the literature.

Barton and Choubey [*13*] proposed 10 standard roughness joint profiles in an article and gave the JRC inverse value of these joints when they are sheared from left to right as shown in Fig. 1.

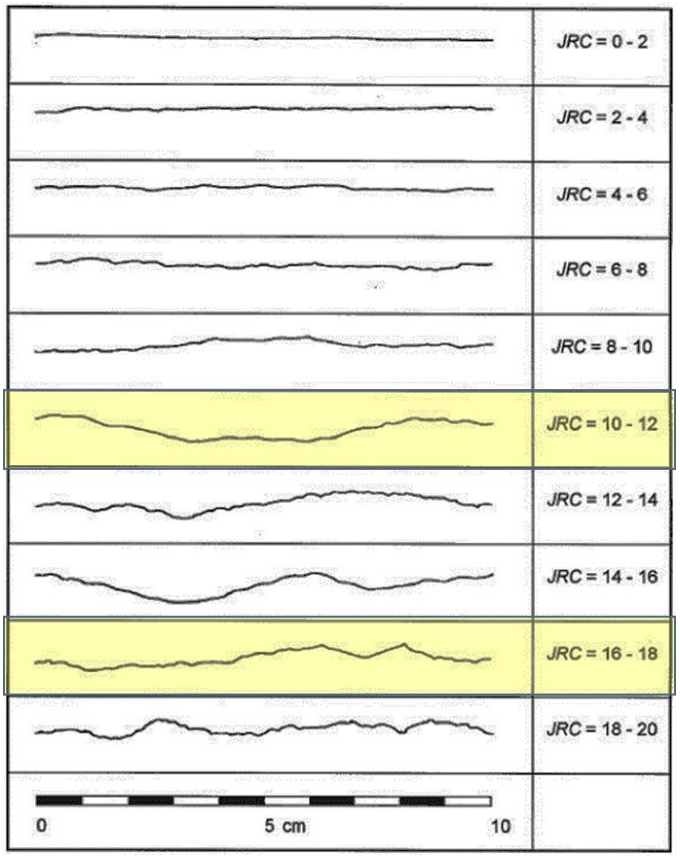

Fig. 1 Roughness profiles corresponding to the joints showing the typical range of JRC values (after [*13*])

Kim et al. [*11*] created the artificial joint of JRC 12 and 17, as indicated in yellow shade in Fig. 1. They used the random midpoint displacement method to manufacture the artificial joint model using a 3D printer. The applied random midpoint displacement method extends the two-dimensional Brownian profile to three dimensions to produce surface roughness [*14, 15*].

Fig. 2 shows the examples of the fabricated joint surface with roughness for 0.13(W) × 0.06(L) m specimens using the 3D printer. We replicated them in the 3DEC model by importing the 3D geometries as illustrated in Fig. 3.

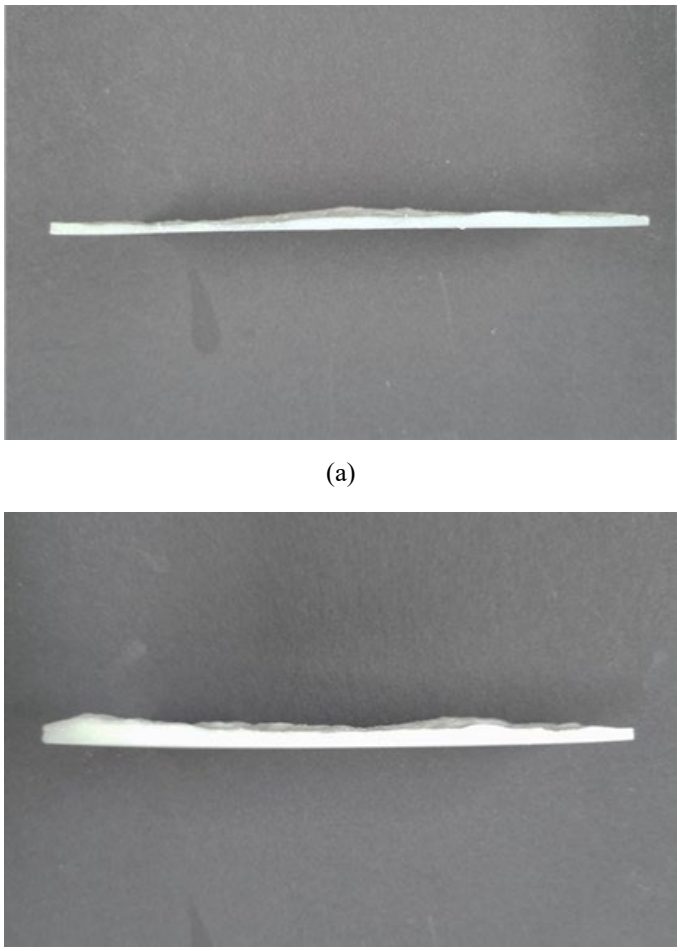

(a)

(b)

Fig. 2. Fabricated roughness on synthetic joint surface – (a) JRC=12; (b) JRC=17 [*11*].

Two deformable synthetic blocks were prepared in the 3DEC model by importing the fabricated block geometries. The two elastic blocks were separated by a continuously yielding joint.

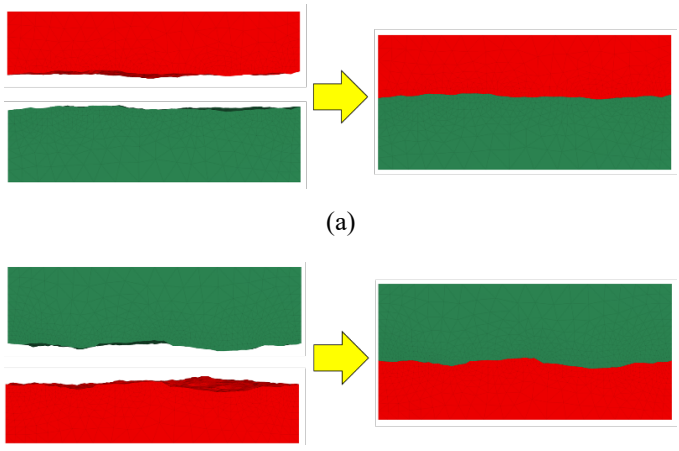

(a)

(b)

Fig. 3. Replicated joint surfaces in 3DEC blocks – (a) JRC=12; (b) JRC=17.

The boundary conditions were Constant Normal Stiffness (CNS) in the direct shear test simulations. The CNS boundary condition is a shear test method in which the normal load constantly increases due to vertical expansion as the test frame applies shear displacement [*16*]. The bottom, the front, and the back of the model were fixed in z- and y-direction, respectively. Both sides of the model were free so that the model was able to move laterally under a given loading condition.

Material properties of the models were determined in static direct shear tests by calibrating the model so that results agreed with the empirical Barton and Bandis equation [*17*]. Table 1 presents the input parameters used for the direct shear simulations in 3DEC.

Table 1. Initial material properties for the 3DEC model

Input parameter	Value
Unit weight (MN/m3)	0.027
Block Young's modulus (GPa)	38.7
Block Poisson's ratio	0.3
Joint normal stiffness (GPa/m)	60
Joint shear stiffness (GPa/m)	50

After the static model calibration, subsequent dynamic numerical direct shear tests were performed using 3DEC to simulate the dynamic direct shear tests performed in the laboratory [*11*].

The dynamic stress determined by the laboratory test as the input for the dynamic shear test simulation is presented in Fig. 4. The dynamic load as velocities calibrated by the laboratory dynamic tests were applied on the right along the top half of the model.

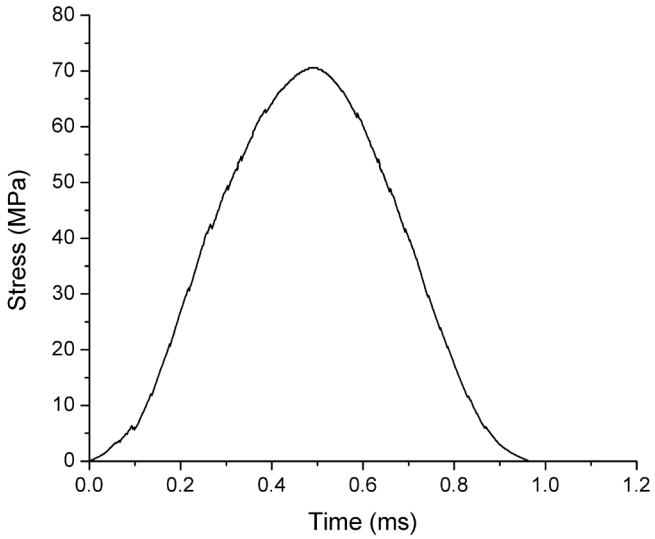

Fig. 4. Dynamic load as input for dynamic shear test simulation.

3. RESULTS AND DISCUSSION

Based on the static direct shear test, the results of shear stress shear displacement curves of joint samples with different roughness are given in the following figures. Here, only the condition of normal stress 0.5 MPa and 3 MPa were taken as a representative for discussion.

Fig. 5 and Fig. 6 illustrate the displacement results of the direct shear test in the 3DEC model for the JRC, which are 12 and 17, respectively. The shear stress/displacement curves are indicated in black in the figures. The x-axis in the figures is a shear displacement in 10^{-3} m and the y-axis in the figures is a shear stress in MPa, respectively. With the increase of JRC and normal stress, the shear stress of joints showed an obvious increasing trend. This behavior was consistent with physical experiments.

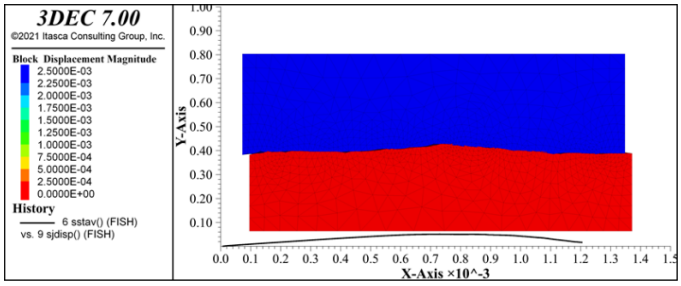

(a)

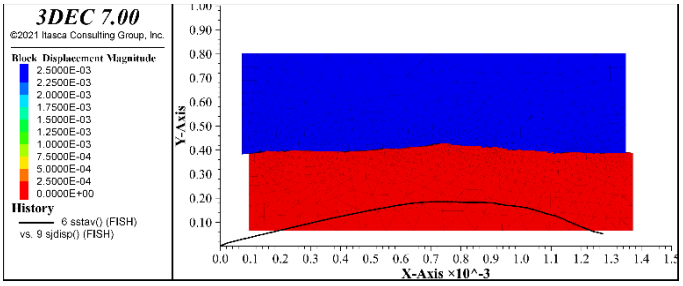

(b)

Fig. 5. 3DEC direct shear test results of synthetic joint with JRC=12 under static condition – (a) normal stress = 0.5 MPa; (b) normal stress = 3 MPa.

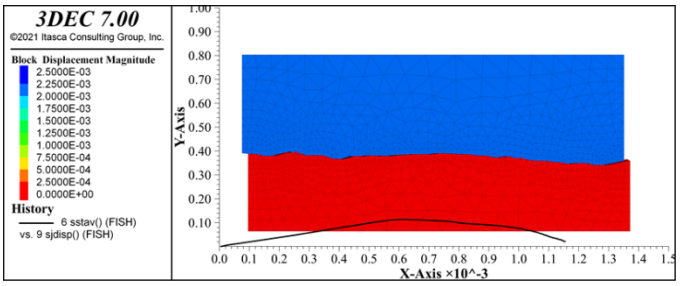

(a)

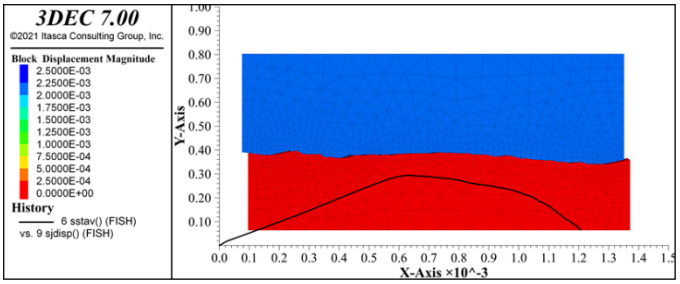

(b)

Fig. 6. 3DEC direct shear test results of synthetic joint with JRC=17 under static condition – (a) normal stress = 0.5 MPa; (b) normal stress = 3 MPa.

In order to proceed to the next step of a dynamic direct shear test simulation, we verified the material properties as the input data for the simulation by calibrating the peak shear stress as a function of the given normal stress obtained from the model with the analytical solution [*17*].

Fig. 7 and Fig. 8 present the comparison of the 3DEC simulation results with the analytical solution. The model results matched well to the analytical solution in terms of the peak shear stress under the normal stress.

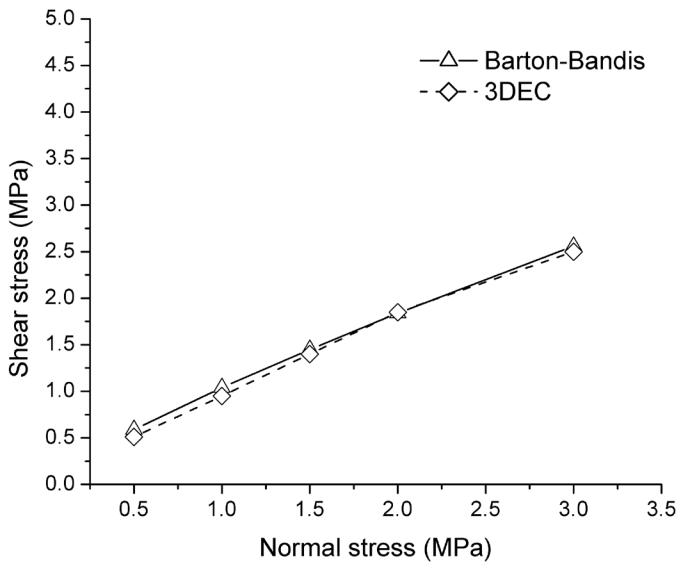

Fig. 7. Peak shear stress versus normal stress obtained from 3DEC model for JRC=12 comparing with analytical solution.

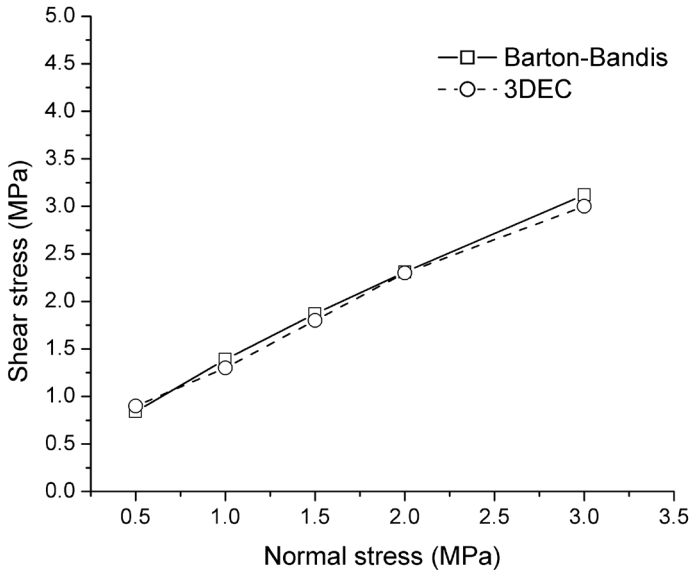

Fig. 8. Peak shear stress versus normal stress obtained from 3DEC model for JRC=17 comparing with analytical solution.

We concluded that this static direct shear test model considering the JRCs in 3DEC was ready to be utilized for a numerical model simulating a dynamic shear test simulation based on the calibrated material properties.

As mentioned above in Fig. 4, we considered the dynamic loading which was determined by the laboratory test to the 3DEC model configuration.

Fig. 9 and Fig. 10 present the displacement results of the dynamic direct shear test in the 3DEC model for the JRC, which are 12 and 17, respectively. The shear stress/displacement curves are indicated in black in the figures. With the increase of JRC and normal stress, the dynamic shear stress showed an obvious increasing trend. This behavior also agreed well with the physical experiments.

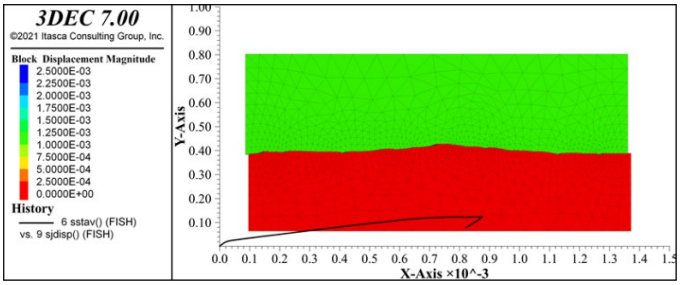

(a)

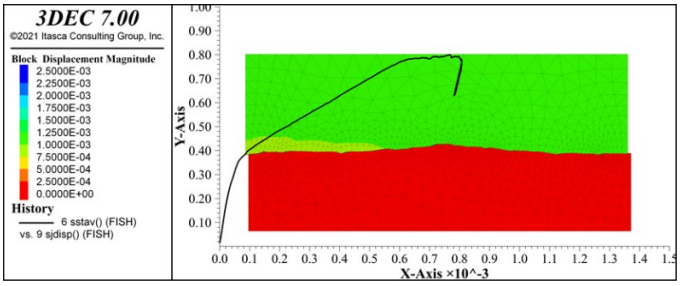

(b)

Fig. 9. 3DEC direct shear test results of synthetic joint with JRC=12 under dynamic condition – (a) normal stress = 0.5 MPa; (b) normal stress = 3 MPa.

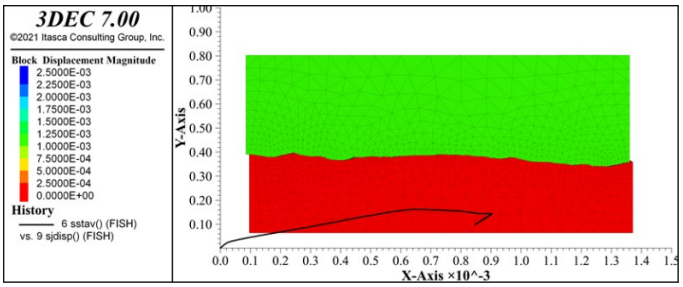

(a)

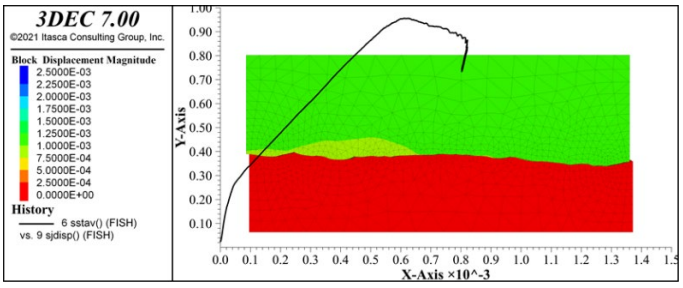

(b)

Fig. 10. 3DEC direct shear test results of synthetic joint with JRC=17 under dynamic condition – (a) normal stress = 0.5 MPa; (b) normal stress = 3 MPa.

We found that the maximum shear stress with the increase of joint JRC was more than two times greater than the result of the static direct shear test in the model. This means that the resistance of the joint roughness to dynamic loading was much stronger than that of the static condition as the JRC increased.

As a result, we confirmed that the ratio of dynamic to static shear strengths vary between approximately 2 and 3 in the range of normal stresses used in the tests as summarized in Table 2.

Table 2. Ratio of dynamic to static shear stress as a function of JRC and normal stress

Normal stress (MPa)	Shear stress ratio (dynamic/static)	
	JRC=12	JRC=17
0.5	2.4	1.8
1	2.1	2.2
1.5	2.9	2.8
2	3.2	3.3
3	3.2	3.2

4. CONCLUSIONS

Researchers from the National Institute for Occupational Safety and Health (NIOSH) conducted a numerical simulation for the purpose of understanding the shear behavior of a joint associated with two different 3-dimensional geometries under both static and dynamic conditions.

In this paper, we report the preliminary results of an ongoing study. We performed static direct shear test simulations for the purpose of calibrating our models with the empirical solution. Afterward, we conducted dynamic direct shear test simulations using 3DEC for the purpose of learning more about the dynamic shear failure mechanisms. The simulations results compared well with those of the laboratory tests.

Further experiments are planned that will test more extreme values of JRC to examine whether the strength ratios will remain in the current range or manifest outside of that generally expected range. Such experiments will provide important information that affects the design of support systems to withstand dynamic stresses that could potentially be applied in underground mines. The results are expected to guide the design of support systems to reduce injuries and fatalities in underground mines.

ACKNOWLEDGMENT

The authors greatly appreciate the help of Drs. Sangho Cho and Gyeongjo Min at Jeonbuk National University in South Korea who made this work possible.

DISCLAIMER

The findings and conclusions in this report are those of the author(s) and do not necessarily represent the views of the National Institute for Occupational Safety and Health. Mention of any company or product does not constitute endorsement by NIOSH.

REFERENCES

1. Kim, Bo-Hyun, and Mark K. Larson (2018) Development of a fault-rupture environment in 3D: A numerical tool for examining the mechanical impact of a fault on underground excavations. *Proceedings of the 37th International Conference on Ground Control in Mining*. (Morgantown, WV: July 24–26, 2018) Englewood, CO: Society for Mining, Metallurgy, and Exploration (SME), pp. 98–111.
2. Kim, Bo-Hyun, and Mark K. Larson (2019) Development of a 3D numerical tool for assessing the mechanical impact of a fault-rupture by normal fault on underground excavations. *Proceedings of the 53rd U.S. Rock Mechanics/Geomechanics Symposium*. (New York: June 23–26, 2019) Gonçalves da Silva, B., et al. eds., ARMA 19–037, Alexandria, VA: American Rock Mechanics Association (ARMA), 8 pp.
3. MSHA (2020) Mine data retrieval system, Mine Safety and Health Administration (MSHA), U.S. Department of Labor, <https://www.msha.gov/mine-data-retrieval-system> [Accessed January 21, 2022].
4. Mauck, H. E. (1958) Coal mine bumps can be eliminated, *Mining Eng.,* Vol. 10, No. 9, 1958, p. 923.
5. Peperakis, John (1958) Mountain bumps at the Sunnyside Mines, *Mining Eng.,* Vol. 10, No. 9, 1958, pp. 982–986.
6. Agapito, Joe F. T., and Rex R. Goodrich (2000) Five stress factors conducive to bumps in Utah, USA, coal mines. *Proceedings: 19th International Conference on Ground Control in Mining*. (Morgantown, WV: August 8–10, 2000) Morgantown, WV: West Virginia University, pp. 93–100.
7. Maleki, Hamid, and Brian White (1997) Geotechnical factors influencing violent failure in U.S. mines. *Proceedings: International Symposium on Rock Support — Applied Solutions for Underground Structures*. (Lillehammer, Norway: June 22–25, 1997) Oslo, Norway: Norwegian Society of Chartered Engineers, pp. 208–221.
8. Boler, F. M., S. Billington, and R. K. Zipf (1997) Seismological and energy balance constraints on the mechanism of a catastrophic bump in the Book Cliffs Coal Mining District, Utah, USA, *Int. J. Rock Mech. Min. Sci.,* Vol. 34, No. 1, 1997, pp. 27–43.
9. Mark, Christopher, and Michael Gauna (2015) Evaluating the risk of coal bursts in underground coal mines. *Proceedings: 34th International Conference on Ground Control in Mining*. (Morgantown, WV: July 28–30, 2015) Morgantown, WV: West Virginia University, pp. 47–53.
10. Rice, George S. (1936) Bumps in coal mines—theories of causes and suggested means of prevention or of minimizing effects. *Transactions of the American Institute of Mining and Metallurgical Engineers,* Vol. 119, 1936, pp. 11–39.
11. Kim, G. G., G. J. Min, C. H. Shin, H. R. Kim, S. H. Cho, J. S. Yang, and K. J. Yun (2022) Laboratory test on direct shear behavior of rock joints using a bar drop impact system. *Proceedings, 56th U.S. Rock Mechanics/Geomechanics Symposium*. (Santa Fe, NM: June 26–29, 2022) Blankenship, D., et al. eds., ARMA 2022–734, Alexandria, VA: American Rock Mechanics Association, Inc. (ARMA),, 6 pp.
12. Itasca Consulting Group, Inc., (2019) 3DEC distinct element modeling of jointed and blocky material in 3D. User's guide. version 7.0., Itasca Consulting Group, Inc., <http://docs.itascacg.com/3dec700/3dec/docproject/source/3dechome.html>.
13. Barton, N., and V. Choubey (1977) The shear strength of rock joints in theory and practice, *Rock Mechaincs,* Vol. 10, pp. 1–54.
14. Seo, H. K., and J. G. Um (2012) Generation of roughness using the random midpoint displacement method and its application to quantification of joint roughness, *Tunnel and underground Space,* Vol. 22, No. 3, pp. 196–204.
15. Choi, S. B., S. D. Lee, and S. W. Jeon (2016) Generation of a 3D artificial joint surface and characterization of its roughness, *Tunnel and Underground Space,* Vol. 26, No. 6, pp. 516–523.
16. Indraratna, B., A. Haque, and N. Aziz (1998) Laboratory modelling of shear behaviour of soft joints under constant normal stiffness conditions, *Geotech. Geol. Eng.,* Vol. 16, No. 1, pp. 17–44.
17. Barton, N., and S. Bandis (1990) Review of predictive capabilities of JRC-JCS model in engineering practic. *Proceedings of the International Symposium on Rock Joints*. (Loen, Norway: June 4–6, 1990) Rotterdam: Balkema, A. A., pp. 603–610.